Physics in Medicine 7 (2019) 100015

Contents lists available at ScienceDirect

Physics in Medicine

journal homepage: www.elsevier.com/locate/phmed

Application of multi-channel differential optical density on fast detection of degree of traumatic dural hematoma

Huiquan Wang[a,c], Fang Xia[a], Songlin Yu[b], Zhe Zhao[a,c,*], Jinhai Wang[a]

[a] School of Life Sciences, Tianjin Polytechnic University, 399 Binshui West Street, Xiqing District, Tianjin, 300387, PR China
[b] Tianjin Institute of Metrological Supervision and Testing, 4 Keyanxi Rd., Nankai District, Tianjin, 300192, PR China
[c] Tianjin University, 92 Weijin Road, Nankai District, Tianjin, 300072, PR China

ARTICLE INFO

Keywords:
Traumatic subdural hematoma
Differential near-infrared optical density
Multi-channel differential optical absorbance

ABSTRACT

Due to the advantages of rapid and non-invasive detection of traumatic dural hematoma using near-infrared differential optical density method, this technology has become a hot research topic in tissue optics in recent years and has important applications in clinical emergency treatment. To further improve the detection accuracy of traumatic subdural hematoma degree, in this paper, a multi-channel differential optical density method was used to obtain the bilaterally-symmetric optical density data of brain. A calibration model with the optical absorption coefficient of the brain tissue and the differential optical density was established using the partial least squares method to predict intracranial epidural hematoma. Simulation results show that the average relative error of the absorption coefficient of dural hematoma using the prediction model was 11.16% and the average relative error on hematoma depth prediction was less than 1%. The model meets the demands of noninvasive traumatic subdural hematoma degree detection. By introducing multi-channel differential optical density method into the noninvasive detection of subdural hematoma, the effects of individual differences on the detection result could be eliminated significantly and the detection accuracy of traumatic subdural hematoma degree can be improved.

1. Introduction

Dural hematoma often occurs after traumatic brain injury. The difficulty of accurate and timely diagnosis and treatment can lead to irreversible brain damage and endanger the life of the patient. Therefore, non-invasive detection of traumatic dural hematoma is always a research focus in the biomedical engineer field [1]. Traditional imaging methods such as CT and MRI can display various parts of the brain tissue directly and accurately. However, because of their bulky equipment and high cost, they are not suitable for rapid and timely diagnosis of subdural hematoma right after traumatic brain injury. The near-infrared band from 650 nm to 900 nm is an optical window for biological tissues. Light within this wavelength range can penetrate for a depth of a few centimeters depth into the brain tissue and emit from the surface. By analyzing the emitted light information, the optical properties of the brain tissue can be obtained and rapid non-invasive detection of brain disorders can be achieved [2]. Therefore, near-infrared spectroscopy has been widely used in clinical applications such as brain function imaging [3], brain tumor imaging [4], cerebral blood flow measurement [5] and brain hematoma detection [6].

Britton Chance from the University of Pennsylvania in the US has proposed the determination of cerebral hematoma occurrence by comparing the optical contrast difference between two positions in the brain [7]. This method involves the separate detection and calculation of optical absorbance from two positions in the brain of the same person, and a comparison of the absorbance difference at these two positions. Absorbance differences of 0.15 and over 0.4, correspond to the occurrence of cerebral hypoxia and cerebral hematoma, respectively. R. Salonia, and Bartlomiej et al. have conducted continuous studies on this method [8,9]. To a certain extent, differential optical density can eliminate the influence of individual differences on quantitative detection using near-infrared spectroscopy. However, because of the fixed distance between the detector and the light source, the best information can only be obtained within its effective detection depth [10]. The differences in the structure and the optical parameters of the human head, as well as the differences in the location of hematomas and lesions can cause errors in detection performed using the differential optical density method. This method also cannot quantitatively determine the degree of cerebral hematoma and causes inconvenience in clinical first aid.

* Corresponding author. School of Life Sciences, Tianjin Polytechnic University, 399 Binshui West Street, Xiqing District, Tianjin, 300387, PR China
E-mail address: tjpubme@126.com (Z. Zhao).

https://doi.org/10.1016/j.phmed.2019.100015
Received 11 October 2018; Received in revised form 7 April 2019; Accepted 8 April 2019
Available online 08 June 2019

In this paper, a multi-channel differential optical density method is proposed to detect the degree of cerebral hematoma. Multi-channel sensors located at certain interval distance were used simultaneously to collect and analyze the emitted light signals from the targeted area, and to calculate the differences in optical absorbance at symmetrical positions of the brain. Using the partial least squares method, a quantitative calibration equation for multi-channel differential optical density and the position of cerebral hematoma was established to predict the absorption coefficient of the intracranial dural position and ultimately the degree of cerebral hematoma. Simulation results showed that the detection of the degree of cerebral hematoma in different depths and different anatomical structures of the brain can be achieved by using the multiple-channel differential optical density method, and the individual differences can be effectively eliminated. These results provide strong evidence for the applicability of near-infrared spectroscopy-based rapid detection of the degree of cerebral hematoma in clinical practice.

2. Brain optical model

According to the anatomy of the human brain, the brain model consists of 5 layers, namely, the scalp, skull, cerebrospinal fluid (CSF), grey matter and white matter (Fig. 1). Brain structure and optical parameters at 840 nm wavelength are shown in Table 1 [11,12]. The definitions of the brain parameters are as follows: n is the refractive index, μ_a (cm^{-1}) is the absorption coefficient, μ_s (cm^{-1}) is the scattering coefficient, g is the anisotropic factor, and d (cm) is the tissue thickness, of which d1 is the thickness of the scalp, d2 is the thickness of the skull. These thicknesses are different for different individual and depend on the growing-up environment, their age, race, sex and other factors. In general, (d1 + d2) is usually in the range of 1.0–1.7 cm [13].

Clinical cerebral hematoma can be divided into subdural hematoma, epidural hematoma, intracerebral hematoma and subarachnoid hemorrhage. Most of the hematomas caused by traumatic brain injury are subdural hematoma and are positioned extradurally or intradurally under the skull [14], which is the third layer, i.e. the CSF layer in the brain model. As the head skull thickness changes, the hematoma location changes. When traumatic brain hematoma occurs, the absorption coefficient of the brain tissue increases significantly. Clinical studies have shown that the absorption coefficient increases over 10 times when hematoma occurs, while the normal value of the dural absorption coefficient is 0.05 cm^{-1}. In order to simulate different degrees of hematoma, in this study, the dural position μ_a was set in the range of 0.5–1.5 cm^{-1} and the adjustment step was 0.1 cm^{-1}.

In this study, the photon propagation simulation algorithm was optimized and modified based on the Monte Carlo algorithm by professor Wang Lihong, and the number of photons scattered from the light source and the photon trajectory of each layer were recorded [15]. The number of photons in this simulation was 10^8; the wavelength was 840 nm; the thickness of the scalp and the skull layers were set at 1.0–1.7 cm with a 0.1 cm step. The dural position μ_a was set at 0.5–1.5 cm^{-1} with a 0.1 cm^{-1} step, a total of 88 radial light intensity

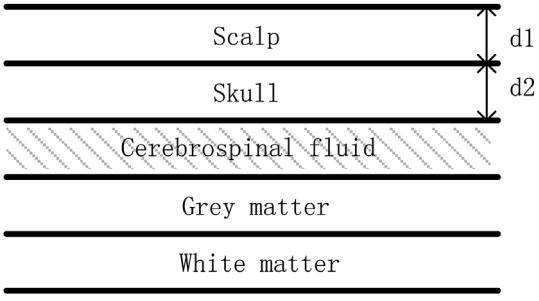

Fig. 1. Structure of brain model.

Table 1
Optical parameters of Brain model at 840 nm.

Brain Layer	n	μ_a (cm^{-1})	μ_s'(cm^{-1})	g	d (cm)
Scalp	1.45	0.21	18.1	0.9	d1
Skull	1.45	0.19	15.2	0.9	d2
CSF	1.45	0.05	2.3	0.9	0.2
Grey matter	1.45	0.42	20.9	0.9	0.4
White matter	1.45	0.17	86.5	0.9	3.4

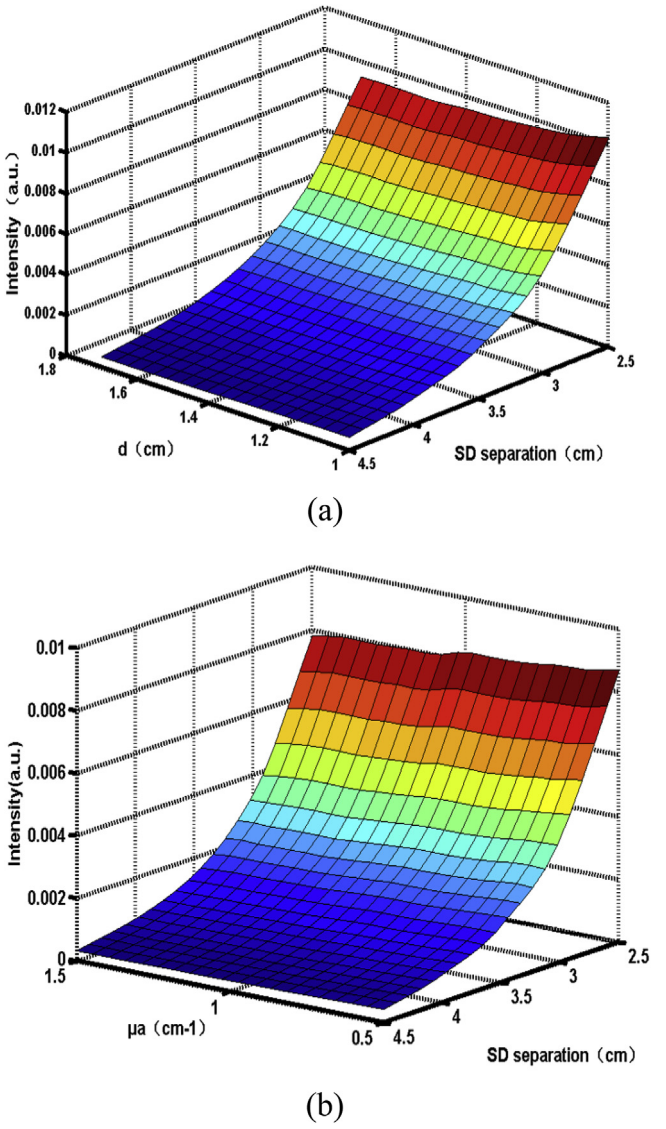

Fig. 2. (a) Light intensity distribution of light source radial with fixed d; (b) Light intensity distribution of light source radial with fixed μ_a.

distribution measurements of the light source were obtained by MC as shown in Fig. 2. The "SD separation" represents the distances of detectors and light source. And Fig. 2(a) shows the light intensity distributions detected by detectors with different distances to the light source when the scalp skull thickness ranged from 1.0 to 1.7 cm and the dural position μ_a was 0.05 cm^{-1}. Fig. 2(b) shows the light intensity distributions detected at different distances to the light source when the scalp skull thickness was 1.3 cm and the absorption coefficient of the dural position μ_a was 0.5–1.5 cm^{-1}. The data shows that there are significant differences in light intensity distribution detected by the fixed-position detectors from different individuals. The detection error would be relatively large if a single fixed-position detector was used.

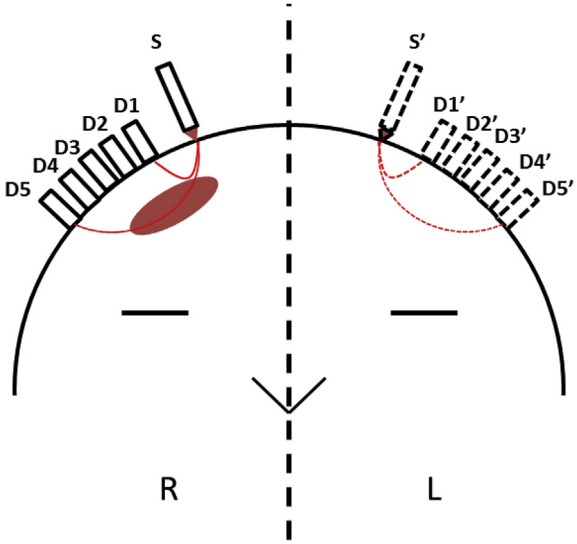

Fig. 3. Multi-channel differential optical density detection.

3. Multi-channel differential optical absorption method

Fig. 3 shows the configuration of a brain hematoma detection scheme using the multi-channel differential optical absorption method. In this figure, S and S′ stand for incident optical sources, while D1-D5 and D1′-D5′ are photoelectric detectors. The detection was conducted at symmetrical positions on the human head. First, the light intensities on the right side of the head (R site) were detected by the 5 detectors and denoted as I_1–I_5;Then, light intensities on the left side of the head (L site) were detected by the 5 detectors and denoted asI_1'–I_5'. I_0 was the incident light intensity for both the left and right sides. By using Equations (1) and (2), light absorbance at each location OD_1-OD_5 and OD_1'-OD_5' can be obtained respectively.

$$OD_i = \log_{10}\left(\frac{I_0}{I_i}\right), (i = 1,2..., 5) \tag{1}$$

$$OD_i' = \log_{10}\left(\frac{I_0}{I_i'}\right), (i = 1,2..., 5) \tag{2}$$

Dividing the light absorbance of the left and right symmetrical locations, the differential absorbance can be calculated as

$$\Delta OD_i = OD_i - OD_i' = \log_{10}\left(\frac{I_0}{I_i}\right) - \log_{10}\left(\frac{I_0}{I_i'}\right) = \log_{10}\left(\frac{I_i'}{I_i}\right), (i = 1,2..., 5) \tag{3}$$

According to the differential absorbance at symmetrical head positions, information on the brain hematoma degree can be obtained. By using the differential absorbance data from multiple positions to establish a model, the accuracy of the detection of the cerebral hematoma can be improved effectively.

4. Hematoma prediction model establishment and results

4.1. Establishment of the prediction model

The partial least squares method (PLS) has strong anti-interference ability. It eliminates noise and extracts useful information efficiently by reducing the model dimensions. A PLS model uses comprehensive information. This model offers strong small-sample regression abilities and the capacity to resist multiple linear interference from independent variables. The 88 data samples obtained in the second section of this paper were used as the raw data. Five detectors were placed at positions 2.5 cm, 3.0 cm, 3.5 cm, 4.0 cm and 4.5 cm from the radial position of the light source respectively. Gaussian white noise with a 1000:1 signal to noise ratio was added respectively to simulate a real data collection situation. The calibration model was established based on the PLS model, using the light intensity distributions from the positions of the 5 detectors, the differential optical absorption, epidural position μ_a and scalp skull thickness d. 72 samples were randomly selected as the modeling sample set and the remaining 16 samples were used as the prediction sample set. By using the cross-validation method for one-by-one elimination and 10 as the estimated total component number, the distribution of the correlation degree of different components R-Sq is shown in Fig. 4. The figure shows that when the component number was 5 in both scalp and skull thickness d prediction model and the epidural position μ_a prediction model, the correlations R-Sq of the model were the best. Therefore, the component numbers for both prediction models were set at Fig. 4.

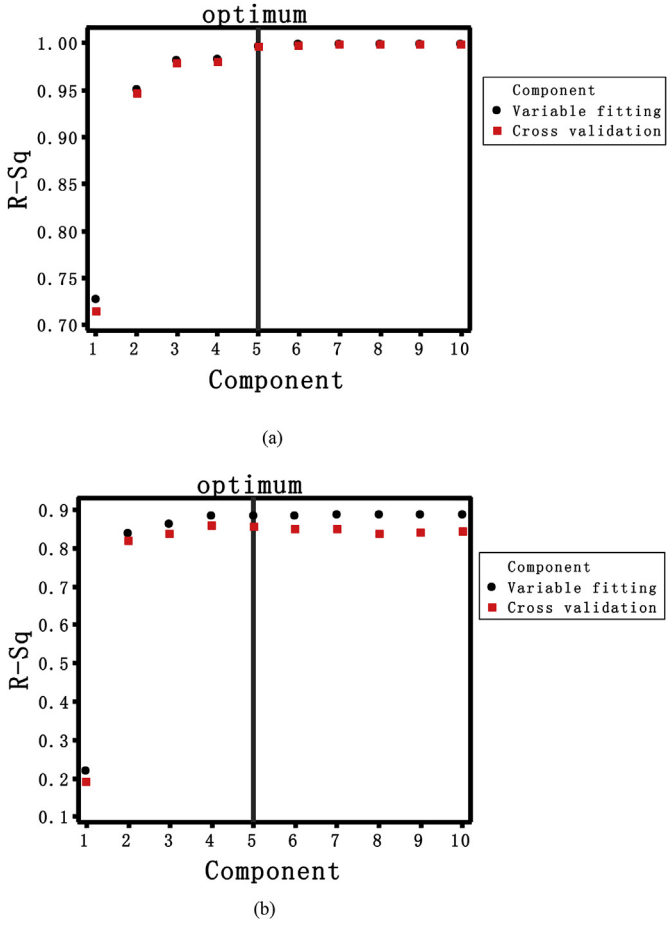

Fig. 4. (a) Optimal component selection of scalp and skull thickness d. (b) Optimal component selection of epidural position μ_a.

4.2. PLS prediction model result

Fig. 5 shows the results from the PLS prediction model on the scalp and skull thickness d, in which the model set prediction correlation was 99.59%; the average error was 0.0108 cm; the maximum error was 0.0318 cm. The prediction set predictive correlation was 99.65%; the average error was 0.0115 cm; the maximum error was 0.0277 cm. Fig. 6 shows the results from the PLS prediction model on the epidural position μ_a, in which the model set's predictive correlation was 88.94%; the average error was 0.0838 cm^{-1}, the maximum error was 0.2593 cm^{-1}; the prediction set's predictive correlation was 86.65%; the average error was 0.1047 cm^{-1}; and the maximum error was 0.2990 cm^{-1}.

In this study, multi-channel differential optical absorbance

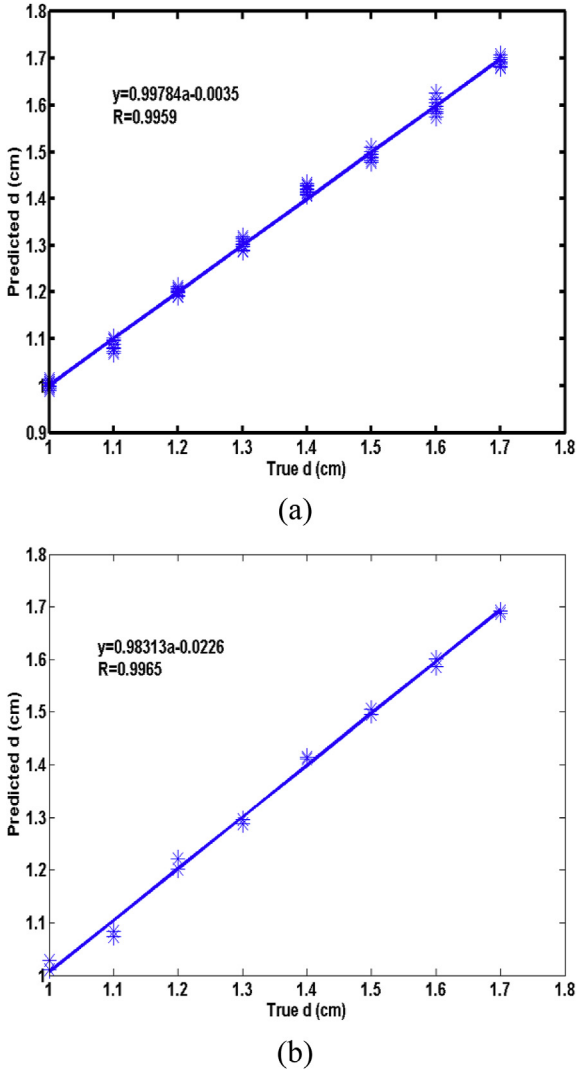

Fig. 5. PLS prediction model on the scalp and skull thickness d. (a) Prediction results of model set; (b) Predictive results of prediction set.

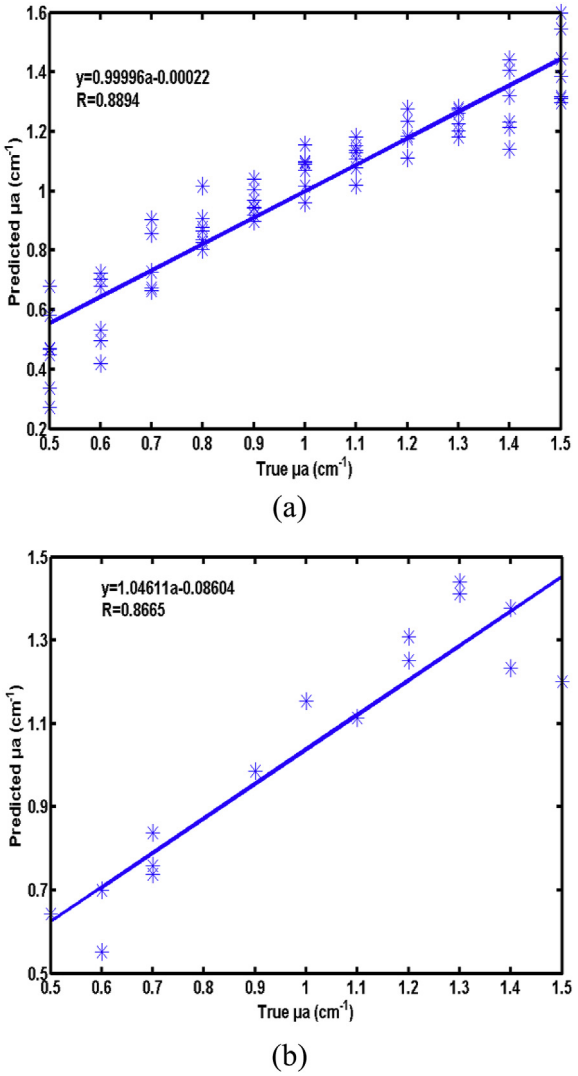

Fig. 6. PLS prediction model on the epidural position μ_a. (a) Prediction results of model set; (b) Prediction results of prediction set.

information and light intensity distribution information were both introduced into epidural location μ_a modeling, so that multi-dimensional data was used effectively and individual differences were eliminated. The prediction accuracy of the model set and the prediction set and the correlation degree between the predicted and real value meet the accuracy requirements of clinical rapid and non-invasive traumatic dural hematoma detection, providing a basis for the rapid detection of brain hematoma based on near-infrared spectroscopy.

5. Conclusion

The scalp and skull thickness reflects the depth of the hematoma, and different epidural positions μ_a reflect the degree of traumatic epidural hematoma. In this study, through the analysis of multi-channel near-infrared differential absorbance and optical intensity distribution, the scalp and skull thickness and epidural position models were established with high prediction accuracy. This basically meets the doctor's needs for a rapid and accurate diagnosis of a patient with traumatic hematoma and making corresponding treatment plans. The model can be used to test traumatic subdural hematoma patients with different scalp and skull thicknesses with good adaptability. It provides an important new reference for rapid detection and degree prediction of traumatic epidural hematoma.

Acknowledgments

The work described in this paper was fully supported by National Natural Science Foundation of China (Grant No. 61705164) and Science and Technology Project of Tianjin (Grant No. 16PTGCCX00120).

References

[1] Tushar Kanti Bera, Noninvasive electromagnetic methods for brain monitoring: a technical review, Brain-Computer Interfaces (74) (2015) 51–95.
[2] Gang Xu, Li Xiao-Li, Liu Xiao-Min, A simple design of functional near-infrared spectroscopy system, Spectrosc. Spectr. Anal. 35 (2) (2015) 552–556.
[3] Mina Nourhashemi, Mahdi Mahmoudzadeh, Fabrice Wallois, Thermal impact of near-infrared laser in advanced noninvasive optical brain imaging, Neurophotonics 3 (1) (2016), https://doi.org/10.1117/1.NPh.3.1.015001.
[4] Saji Uthaman, Joon-suk Bom, Hyeon Sik Kim, Johnson V. John, Hee-Seung Bom, Seon-Jong Kim, Jung-Joon Min, II Kim, In-Kyu Park, Tumor homing indocyanine green encapsulated micelles for near infrared and photoacoustic imaging of tumors, J. Biomed. Mater. Res. B Appl. Biomater. 104 (4) (2016) 825–834.
[5] S. Kato, K. Yoshitani, Y. Ohnishi, Cerebral blood flow measurement by near-infrared spectroscopy during carotid endarterectomy, J. Neurosurg. Anesthesiol. 28 (4) (2016) 291–295.
[6] T. Braun, U. Kunz, C. Schulz, A. Lieber, C. Willy, Near-infrared spectroscopy for the detection of traumatic intracranial hemorrhage: feasibility study in a German army field hospital in Afghanistan, Unfallchirurg (2014), https://doi.org/10.1007/s00113-013-2549-0.
[7] Claudia S. Robertson, Shankar Gopinath, Britton Chance, Use of near infrared spectroscopy to identify traumatic intracranial hemotomas, J. Biomed. Opt. 2 (1)

(1997) 31–41.
[8] R. Salonia, M.J. Bell, P.M. Kochanek, R.P. Berger, The utility of near infrared spectroscopy in detecting intracranial hemorrhage in children, J. Neurotrauma 29 (6) (2012) 1047–1053.
[9] Bartlomiej Tyzo, Michal Rutkowski, Urszula Zielinska, Karolina Thumtyzo, Tomasz Trojanowski, Krzysztof Turowski, Radoslaw Rola, Piotr Trojanowski, Anaplastic ependymoma metastases to the scalp requiring free flap surgeryendymoma metastases to the scalp requiring free flap surgery, Oncol. Clin. Pract. 11 (4) (2015) 215–220.
[10] X.N. Wang, L.I. Wei-Tao, Z.Y. Qian, X.Z. Wang, Near infrared effective detection depth in mouse traumatic brain edma model, Acta Photonica Sin. 40 (2) (2011) 277–281.
[11] C.J. Holmes, R. Hoge, L. Collins, et al., Enhancement of MR images using registration for signal averaging, J. Comput. Assist. Tomogr. 22 (2) (1998) 324.
[12] Shinji Umeyama, Toru Yamada, New cross-talk measure of near-infrared spectroscopy and its application to wavelength combination optimization, J. Biomed. Opt. 14 (3) (2009) 034017.
[13] G.E. Strangman, Z. Quan, L. Zhi, Scalp and skull influence on near infrared photon propagation in the Colin27 brain template, Neuroimage (85) (2014) 136–149.
[14] M. Ross Bullock, Chesnut Randall, Jamshid Ghajar, David Gordon, Roger Hartl, David W. Newell, Servadei Franco, Beverly C. Walters, Jack Wilberger, Surgical management of traumatic parenchymal lesions, Neurosurgery 58 (2006) S25–S46.
[15] Steven L. Jacques, Lihong Wang, Monte Carlo Modeling of Light Transport in Tissues. Optical-Thermal Response of Laser-Irradiated Tissue, (1995), pp. 73–100.